# Chemical effect of sewage sludge ash on early-age hydration of cement used as supplementary cementitious material

Zhiyang Chang[a], Guangcheng Long[a]*, Youjun Xie [a], John L Zhou[a,b]

[a]School of Civil Engineering, Central South University, 68 Shaoshan South Road, Changsha, Hunan 410075, China

[b]School of Civil and Environmental Engineering, University of Technology Sydney, Sydney, NSW 2007, Australia

*Corresponding author:

Email address: longguangcheng@csu.edu.cn (G. Long)

## Abstract

For a full understanding of chemical effects of calcined sludge ash on early-age cement hydration, hydration heat evolution, solid and aqueous composition of cement blended with sludge ash were investigated. The Al dissolution of S600 ash promoted the formation of ettringite and consumption of gypsum resulting in a high initial hydration heat. However, high concentrations Al and Si caused by continuous dissolution of Al and Si in ash inhibited significantly the $C_3S$ dissolution. Interestingly, S800 ash had little effect on early cement hydration as higher calcination temperature decreased Al activity. Despite a delay in the induction period, the potential pozzolanic reaction of S800 ash compensated the dilution effect and contributed to more hydration heat and hydrates. Thus, S800 ash is feasible to be used as supplementary cementitious material. Further studies are recommended to focus on the long-term performance of cement paste blended with sludge ash.



*Keywords*: sewage sludge ash; chemical effect; cement hydration; phase assemblage; aqueous composition.

## 1. Introduction

Sewage sludge is the solid residual of wastewater treatment. A large amount of sludge is generated with the rapid development of urbanization and its disposal is becoming an urgent and inevitable issue [1]. The enhanced public awareness of environmental protection has put pressure on traditional disposal techniques such as landfilling, compost and ocean dumping [2]. Incineration is regarded as one of the most environmental-friendly disposal options which reduces sludge volume by up to 65% [3-4]. The construction industry provides a valorization alternative for incineration remaining ash to be used as a supplementary cementitious material (SCM) [5-8].

Cement industry is a dominant contributor of energy consumption and $CO_2$ emissions [9]. The application of SCMs to partially replace cement in the production of building materials will reduce $CO_2$ emissions and bring remarkable economic benefits. SCMs are generally composed of amorphous phases such as soluble aluminosilicates, siliceous and calcium aluminosilicates. For example, coal fly ash, silica fume and ground blast furnace slag are frequently-used SCMs since they are pozzolanic or self-cementing [10-12]. Incinerated sewage sludge ash has a similar chemical composition to coal fly ash, as both contain high proportion of $SiO_2$, $Al_2O_3$ and CaO [13].

Many researchers have explored potential applications of incinerated sludge ash reused as a SCM in building materials [14-19]. The irregular morphology and high specific surface area of sludge ash increase water demand and reduce the workability of fresh mortars significantly [20-21]. The addition of superplasticizer could compensate the workability loss caused by sludge ash [20-21]. Currently, the effect of sludge ash on the cement hydration and setting time has not yet reached a consensus. Some researchers suggest that sludge ash induced a delay of cement hydration due to the dilution effect and minor elements in ash [20], or the presence of the phosphorus in ash[16,22-23]. Conversely, other studies show that the filling effect of sludge ash accelerated hydration reaction [18,24]. The differences in sludge sources and heat-

treatment methods make physicochemical properties of sludge ash distinguishable from each other. Therefore, they might present different influence on cement hydration. The pozzolanic reactivity of sludge ash has been confirmed by previous studies which is highly related to its fineness [25]. Despite a decrease in early compressive strength of mortar with sludge ash addition, the potential pozzolanic reactivity of sludge ash contributed to long-term development of strength. There is no significant difference in the mechanical strength and shrinkage of mortar with 10% substitution of cement by sludge ash [15,26]. Even at a 20% replacement level, the compressive strength of test mortar decreased merely by 4.5 % at 90 days which was far superior to the ASTM C618 limit [18]. Apart from the common hydrated products of cement, there are brushite and aluminum-rich hydrates in sludge ash-derived cement pastes. Brushite is generated from the reaction of phosphorus compounds in sludge ash and calcium hydroxide in solution, which contributes to the strength development of mortar [22,27-28]. The additional aluminum released from sludge ash increases the amount of Al-bearing hydrates, such as ettringite and calcium aluminosilicate hydrates [16,24].

The durability of sludge ash-fabricated products should be paid more attention as they are applied to engineering facilities. A study reported that the co-combustion ash of sewage sludge and rice husk had a negative effect on freeze-thaw (F-T) durability of cement-based products due to the prevention for pozzolanic reaction by F-T action [29]. The effect of sludge ash on the pore structure of paste was found negligible at 10% replacement level in comparison to the control but the porosity was increased with sludge ash substitution up to 30% [15,18]. Corrosion resistance in reinforcement of mortars with 10% sludge ash exhibited comparable steel corrosion rate to the control mortars [30]. Based on the review of relevant literature, it is observed that 10% cement substitution by sludge ash might be a safe threshold from the standpoint of durability. In addition to durability, there is concern about environmental impact of sludge ash-amended construction products due to the nature of sewage sludge. During the toxic characteristic leaching procedure (TCLP), the majority of sludge ash-containing mortars and concrete samples showed toxic chemicals far below the regulatory limits [14,20,29,31-33]. On the one hand, calcination process incorporates

heavy metal ions into the amorphous or crystal structure of sludge ash [34]. On the other hand, the heavy metals could be embedded into the structure of hydration products in cement paste [35-36]. Therefore, the utilization of sludge ash in construction materials should not present pollution leaching problem.

Most research concentrates on the workability and mechanical strength of sludge ash-amended products, such as mortars and concrete. Despites the satisfying results of the sludge ash as SCM, there is still little information available about its chemical effect on cement hydration and hydration mechanism, especially at early age. Generally, sludge ash consists of a high proportion of amorphous $SiO_2$ and $Al_2O_3$. As reported in literature, aluminium has a significant influence on cement hydration evolution, especially for $C_3S$ [37-38]. Thus, the chemical effect of sewage sludge ash on early-age hydration of Portland cement should be determined fully in consideration of aluminate and silicate phases in ash. Under this purpose, the physical and chemical properties of two sludge ashes calcined at 600 ℃ and 800 ℃ were studied. Then the hydration heat evolution, solid phase assemblage and pore solution composition of blended pastes with sludge ash were investigated at various hydration times from 0.5 hour to 168 hour.

## 2. Materials and methods

### *2.1 Materials*

Portland cement (Type P·I 42.5) produced by Fushun Cement Incorporated Company was used in this work. In order to eliminate the dilution effect of sludge ash, the finely ground quartz with a similar particle size distribution to sludge ash was used. The chemical compositions and physical properties of the used materials are listed in Table 1. The particle size distributions of raw materials are shown in Fig. 1.

Sewage sludge was collected from a local sewage treatment plant in Changsha. The sludge was dried at 105℃ for 24h and milled by ball grinder. The sludge ash was obtained from pulverized sludge calcined at 600 ℃, 700 ℃, 800 ℃ and 900 ℃ in a high-temperature furnace and named as samples S600, S700, S800 and S900. The morphology and mineral composition of sludge ash are presented in Fig. 2 and Fig. 3.

**Table 1**

Chemical compositions and physical properties of raw materials

| Material | Cement | Quartz | Sludge | S600 | S800 |
|---|---|---|---|---|---|
| | Chemical analysis (% by mass) | | | | |
| $SiO_2$ | 20.58 | 99.47 | 36.43 | 44.71 | 45.95 |
| $Al_2O_3$ | 4.97 | 0.43 | 17.92 | 25.55 | 25.61 |
| CaO | 63.57 | 0.03 | 2.00 | 2.12 | 2.08 |
| $Fe_2O_3$ | 3.58 | 0.04 | 7.61 | 8.33 | 8.46 |
| MgO | 2.29 | -- | 0.98 | 1.46 | 1.51 |
| $Na_2O$ | 0.53 | -- | 0.15 | 0.19 | 0.28 |
| $K_2O$ | -- | 0.02 | 2.41 | 2.83 | 2.87 |
| $P_2O_5$ | -- | -- | 4.60 | 5.90 | 5.93 |
| $SO_3$ | 2.00 | -- | 1.37 | 0.92 | 0.42 |
| Loss | 1.40 | 0.02 | 44.70 | 6.01 | 1.59 |
| | Physical characteristics | | | | |
| Density | 3.12 | 2.65 | 2.84 | 2.62 | 2.71 |
| $D_{50}$ (μm) | 14.34 | 13.23 | 9.89 | 10.61 | 11.54 |
| BET surface area ($m^2/g$) | 3.5 | 18.60 | 23.20 | 22.12 | 14.51 |

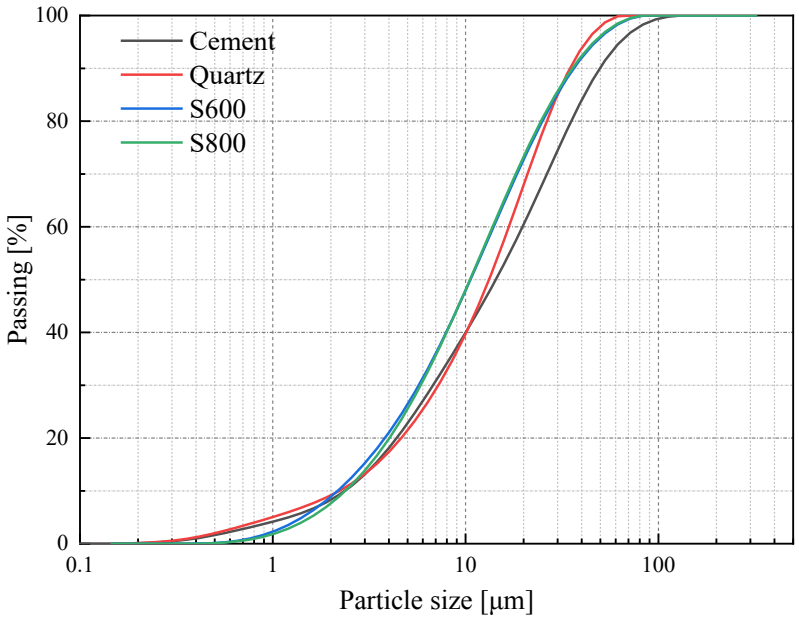


**Fig. 1** The cumulative particle size distribution of raw materials

## 2.2 Methods

### 2.2.1 Isothermal calorimetry

The hydration heat evolutions of cement pastes were monitored by isothermal calorimeter at 20 ℃. The reference sample was prepared with 100% Portland cement (named 100% PC) and test samples were composed of 80% cement and 20% sludge ash (named 20% S600 and 20% S800). All cement pastes are blended with the same stirring speed and time in order to minimize the experimental error.

### 2.2.2 X-ray diffraction (XRD) analysis

XRD is one of the most common analysis techniques to characterize crystalline powder materials (such as cement). Each crystal phase has its unique X-ray diffraction peak. Thus, the hydration products can be determined qualitatively and quantitatively using XRD analysis. The cement pastes for solid and aqueous composition analysis were prepared with 30% cement replaced by quartz powder or sludge ash (named as the Reference, 30% S600 and 30% S800, respectively).

### 2.2.3 Thermogravimetry (TG) analysis

The mass loss of cement sample is monitored continuously by thermogravimetry test from room temperature to 1000 °C. The hydration products can be identified and calculated their content according to the specific decomposition temperatures. In this study, the thermogravimetric analysis on cement pastes is carried out by the synchronous thermal analyzer (STA449C) with a heating rate of 10 °C/min in nitrogen atmosphere.

### 2.2.4 Aqueous composition analysis

There are two methods to collect the pore solution of cement paste. For the slurry before initial setting, a vacuum filtration device was used to extract the pore solution. For the hardened paste, the pore solution was obtained by pressing pastes with a high-pressure extrusion device. The analysis of element (Ca, Si, S, Al, Na and K) of collected pore solution was conducted by ICP-OES. The pH value of the solution was measured using a pH meter.

### 2.2.5 Scanning electron microscopy (SEM) analysis

The morphology of sludge ash was examined using a scanning electron microscopy (QUANTA FEG250). The backscattered electron micrograph (BSE) is often used to observe the microscopic appearance and identify different phases based on the gray-scale characteristics of the image. The BSE images of cement pastes were taken to analyze the microstructure of paste with sludge ash and the reaction degree of cement clinker.

## 3. Results

### *3.1 Characterization of sewage sludge ash*

The particle size distributions of sludge ashes are shown in Fig. 1. The average particle size of S600 and S800 is 15.52 μm and 15.36 μm respectively, smaller than that of Portland cement (21.10 μm). As shown in Fig. 2, the sludge ash particles present irregular morphology with rough surface. The loose and porous layered structures result in their significantly larger BET specific surface area than cement (Table 1).

The main oxides of sludge ash are $SiO_2$, $Al_2O_3$, $Fe_2O_3$ and a small amount of CaO (see Table 1). Abundant organic matter in sludge leads to a high content of $P_2O_5$ (>5%) in incineration ash. The XRD patterns of raw sludge and sludge ash are shown in Fig. 3. The main mineral components are quartz, muscovite, kaolin, dolomite and magnetite. After high temperature calcination, kaolin has been completely decomposed and disappeared in sludge ash [39]. When the calcination temperature rises to 800 ℃, a thermal decomposition of muscovite happens and a part of muscovite is transformed into amorphous siliceous or siliceous-aluminous phases in this stage [39]. In order to determine the content of amorphous phases in sludge ash, 20% ZnO is used as an internal standard in the XRD-Rietveld analysis. As calculated from XRD results, the contents of amorphous phases in S600 and S800 ash are 27.25% and 46.87% respectively, providing the sources of reactive substances for potential pozzolanic reaction. The higher calcination temperature is conducive to formation of amorphous phases. In addition, calcium aluminate is generated from the reaction of calcium and aluminum phase in S800 ash.

In order to determine the dissolution degree of reactive matter such as the soluble aluminum and silicon phases in sludge ash, 0.6 M NaOH+ saturated $Ca(OH)_2$ solution was used as to dissolve sludge ashes with a liquid-to-solid ratio of 100. The Al and Si concentrations in solution and pH value were measured after dissolving for 72 hours. The measured results are shown in Fig. 4. The pH values of the solutions were between 13.3 and13.4. The dissolved Al concentration decreased with the elevated calcination temperature while the Si concentration was on the contrary. The maximum Al concentration was around 24.72 mM in the solution with S600 and that of the solution with S800 was only 14.48 mM. The Al dissolution degree of S600 and S800 was 49.3% and 28.9% respectively. Due to the significant influence of calcination temperature on the physical and chemical properties of sludge ashes, two sludge ashes (S600 and S800) were used to investigate chemical effects on the early hydration of cement in this study.

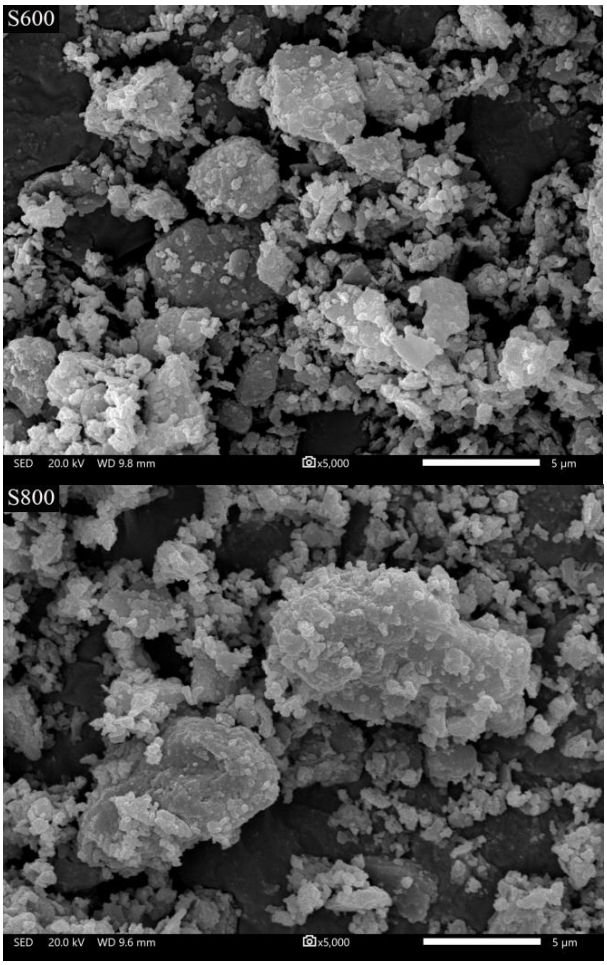


**Fig. 2** SEM image of sewage sludge ash

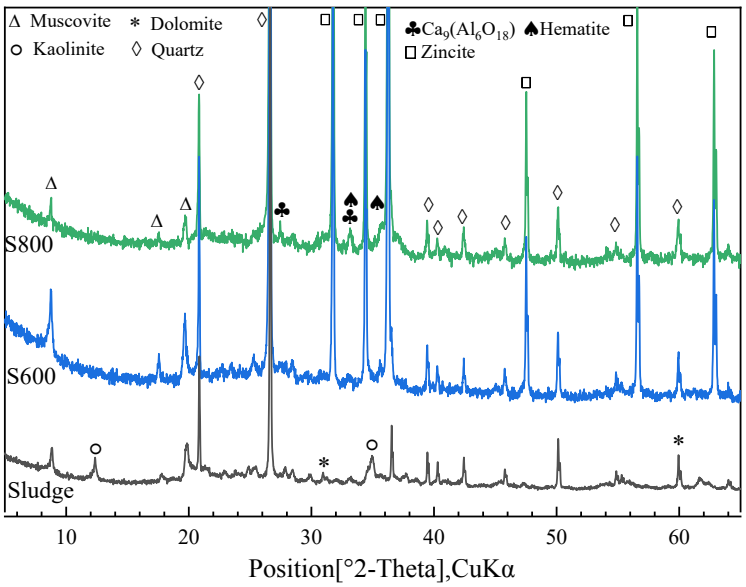


**Fig. 3** XRD pattern of the used sewage sludge and sludge ash

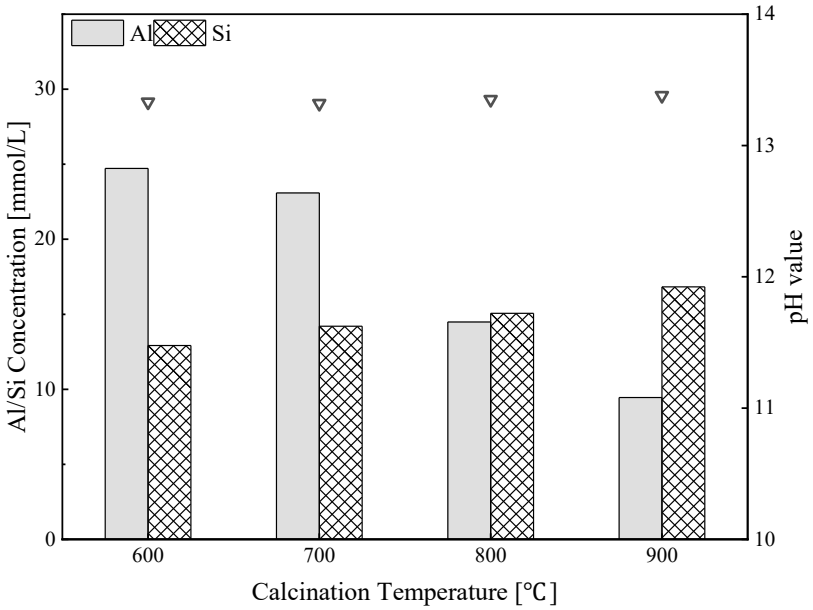


**Fig. 4** The dissolved ion concentrations and pH values of solutions with sludge ash.

*3.2 Hydration process*

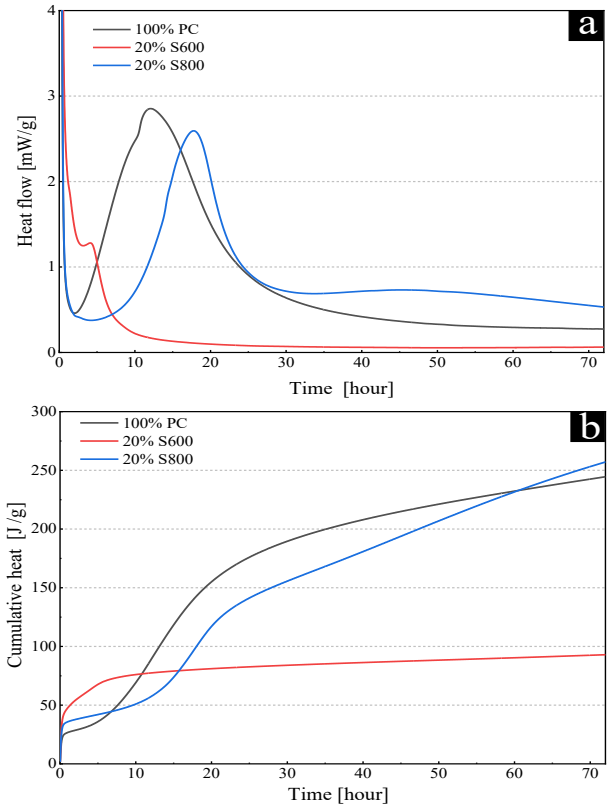


Fig. 5 Heat flow (a) and cumulative heat (b) curves of paste samples (normalized to the amount of cement)

The heat flow and cumulative heat curves of the reference and sludge ash-containing pastes are shown in Fig. 5. In a typical heat evolution curve of cement paste, it can be divided into four periods based on hydration exothermic rate including initial period, induction period, acceleration period and deceleration period. The first peak of the reference (100% PC) appeared at around 12 h of hydration with the maximum heat flow of 2.85mW/g. The paste containing 20% S800 ash presented a similar trend of heat evolution to the reference but its induction period was delayed about 4 hours corresponding to a retardation of alite ($C_3S$) hydration. The heat peak of 20% S800 paste was lower than that of 100% PC. During the deceleration period of 20% S800 paste, a second mild exothermic peak occurred at 40 h~ 60 h which was higher than that of the control. It was indicated that there was another reaction between sludge ash and cement except for the hydration of cement. As seen in Fig. 5 (b), the addition of S800 ash increased the initial heat release. In the first hour of hydration, the cumulative heat of the 20% S800 paste increased rapidly up to 35.78 J/g while a plateau was shown

in the next 10 hours. The hydration heat increased again at 12 h paralleling to the control. After 60 h of hydration, the cumulative hydration heat of 20% S800 paste exceeded that of 100 % PC due to the pozzolanic reaction from sludge ash.

There were significant differences in the hydration heat evolution of the paste with 20% S600 ash compared to the other two samples. The induction period emerged early at 2.5 h of hydration for the 20% S600 paste with a peak value of 1.28mW/g. After 10 hours, a very low heat release rate was maintained until the end of hydration heat test. It can be seen from Fig. 5(b) that the addition of S600 also increased the initial hydration heat of the paste. In the first 6 h of hydration, the cumulative heat of the 20% S600 paste reached 70.71 J/g but it was increased stagnantly later for a long time. The high initial cumulative heat of 20% S600 paste demonstrated the acceleration effect of S600 for cement hydration at this period. However, the existence of S600 or the hydration products formed at early period hindered obviously the subsequent hydration process of cement. This phenomenon of massive exotherm at initial time has been reported in previous studies [41-42]. The addition of Al phase promoted the reaction of aluminate and sulfate producing ettringite and Al- bearing hydration products. These additional hydrates increased the initial heat release rate of cement and shortened the induction period, but inhibited the hydration reaction of $C_3S$ [41]. The S600 ash used in this study contained 25.55% of $Al_2O_3$ and the Al dissolution degree of it reached up to 49.3% under alkaline conditions. Therefore, the presence of soluble Al phase in S600 caused the early abnormal hydration of cement.

*3.3 Solid phase assemblage*

*3.3.1 XRD patterns*

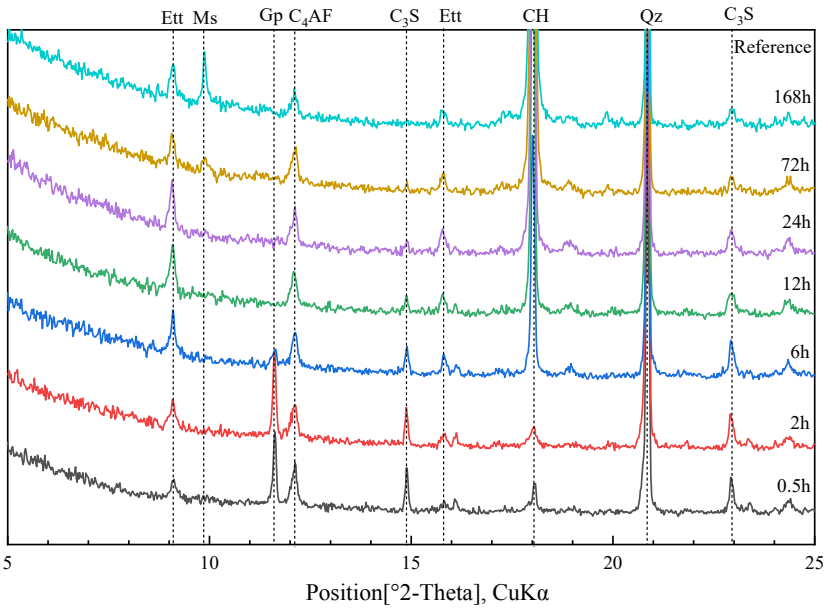
Ett
Ms
Gp
C4AF
C3S
Ett
CH
Qz
C3S
Reference
168h
72h
24h
12h
6h
2h
0.5h
5
10
15
20
25
Position[°2-Theta], CuKα

257

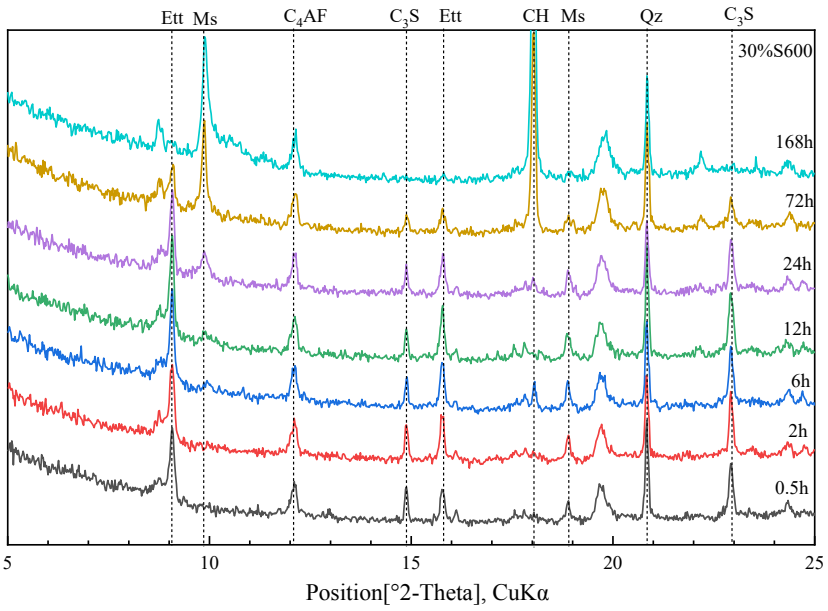
Ett
Ms
C4AF
C3S
Ett
CH
Ms
Qz
C3S
30%S600
168h
72h
24h
12h
6h
2h
0.5h
5
10
15
20
25
Position[°2-Theta], CuKα

258

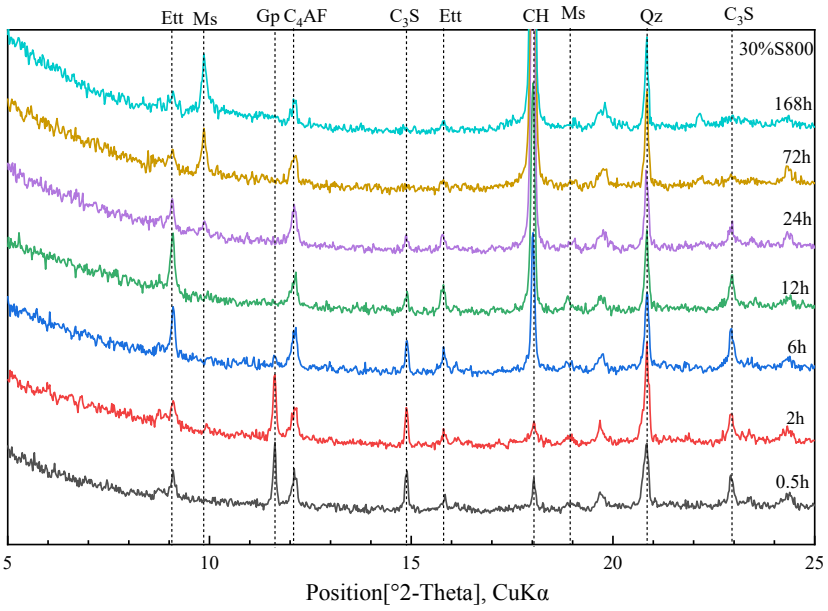


Fig. 6 XRD patterns of (a) reference, (b) 30% S600, and (c) 30% S800 samples at various hydration stages (Ett=ettringite, Ms=monosulfate, Gp=gypsum, CH=portlandite, Qz=Quartz).

The XRD patterns of cement pastes with 30% quartz powder, 30% S600 and 30% S800 sludge ash repectively at different ages are shown in Fig. 6. The primary hydration phases presented in Fig.6 were ettringite (Ett), monosulfate (Ms), portlandite (CH) and gypsum (Gp). Compared with the XRD pattern of the reference, no new hydration product was formed in the existence of S600 and S800 ash. As shown in Fig. 6, the diffraction peak of ettringite was observed in all pastes after 0.5 h of hydration and the peak intensity increased with hydration time. For the reference, the peak intensity of ettringite was reached the highest value at 24 h while it occurred early at 12 h in the pastes with sludge ash. The diffraction peak of monosulfate was detected at 6 h, 24 h and 72 h in the paste of 30% S600, 30% S800 and the reference respectively. At the initial period of hydration, the diffraction peaks of gypsum and portlandite were observed in the XRD patterns of the reference and 30% S800 paste. However, for the 30% S600 paste, gypsum was disappeared and the peak intensity of portlandite was rather weak in the first 24 h.

Generally, the early hydration of Portland cement is controlled by the dissolution

of $C_3A$, $C_3S$ and gypsum. The dissolution and consumption of $C_3A$ and gypsum is related to the formation of ettringite. In 30% S600 paste, gypsum was completely consumed in the first 0.5 h of hydration and the pattern peak intensity of ettringite was obviously higher than that of the other two groups as shown in Fig. 6. It indicated that the depletion of gypsum was caused by the formation of massive ettringite. In the absence of gypsum, ettringite phase is transformed into monosulfate. Thus, the diffraction peak of ettringite decreased gradually after 12 h and disappeared at 168 h with a remarkable peak of monosulfate in 30% S600 paste. In the 30% S800 paste, the moment of this transformation occurred earlier at 24 h than that of the reference. These results illustrated that the sludge ash promoted the transformation from ettringite into monosulfate. It was also can be seen in Fig. 6, the pattern peak intensity of $C_3S$ in 30% S800 paste was decreased faster than that of the reference group after 24 h of hydration. It can be explained by the promotion of S800 ash on the dissolution of $C_3S$.

*3.3.2 TG analysis*

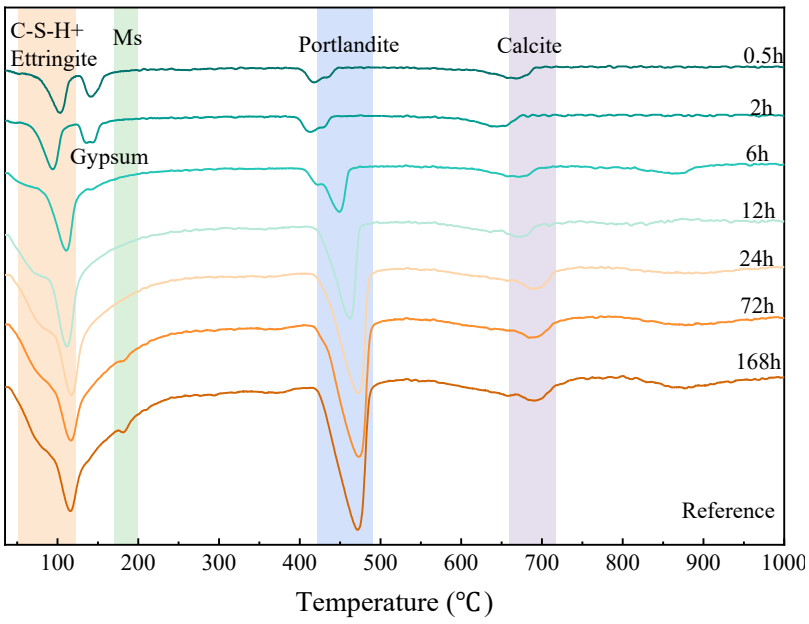

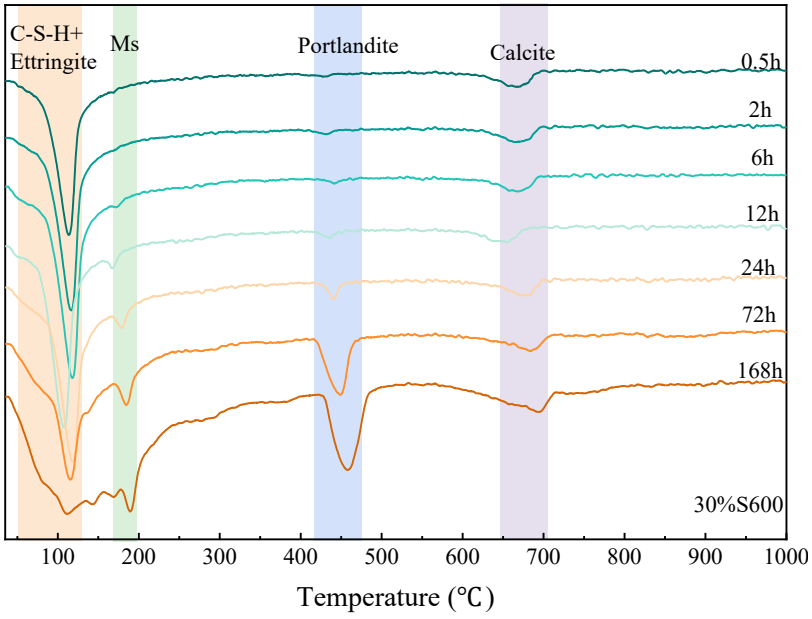


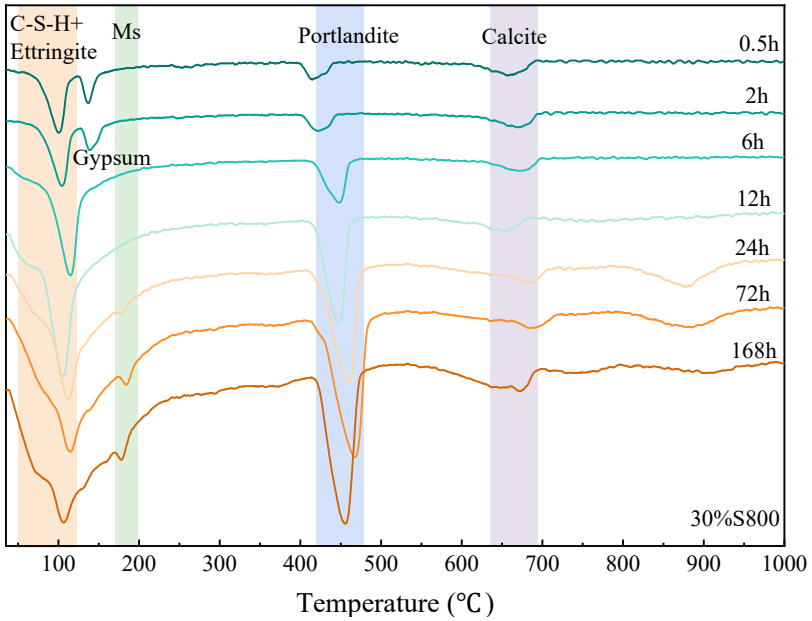


Fig.7 DTG curves of samples at various hydration stages (Ms=monosulfate).

Each type of hydration products has a specific temperature range of decomposition. Thus, the type and content of hydration phases can be identified and calculated accurately according to the TG-DTG curve. The DTG curves of samples at different ages are shown in Fig. 7. In the DTG curve of the reference paste, the first exothermic peak appeared near 100 ℃ corresponding to the dehydration and decomposition of C-

S-H gel and ettringite. The decomposition peak of gypsum occurred at 140 ℃ which disappeared after 6 h of hydration. Monosulfate phase lost interlayer water from structure around 170 ℃ and a weak peak for monosulfate was discerned at age of 72 h. The peak between 400 ℃ and 500 ℃ was induced by the decomposition of portlandite. Compared with the reference, the decomposition peak of C-S-H gel and ettringite was higher in the DTG curve of the 30% S800 paste. The monosulfate peak was also appeared earlier at 24 h. For the 30% S600 paste, the first peak corresponding to the decomposition of C-S-H gel and ettringite was much higher than the other two pastes at 0.5 h. The intensity and shape of the first peak was maintained until 72 h of hydration. The DTG curve of 168 h showed a wider peak shape between 50 ℃ and 200 ℃. At age of 6 h, the peak of monosulfate was observed and the intensity increased with hydration age. Until 24 h of hydration the portlandite peak was discerned in the DTG curve of 30% S600 paste in accordance with the XRD analysis.

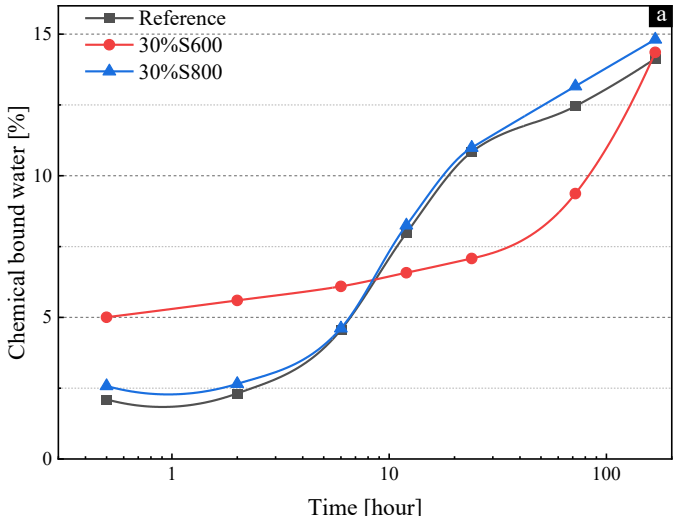

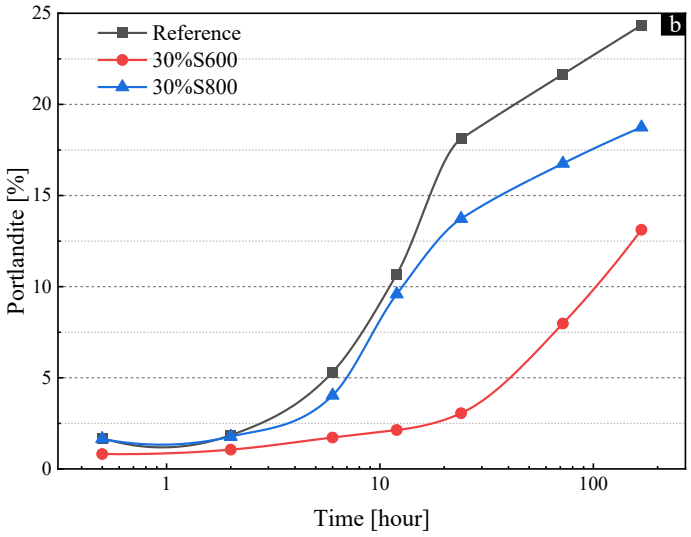


Fig.8 Bound water (a) and portlandite (b) content of paste samples measured by TG and DTG (normalized to Portland cement mass)

The content of chemical bound water (CBW) and portlandite of the pastes at different age were calculated by TG-DTG and the results are shown in Fig. 8. The amount of chemical bound water was determined by the mass loss of sample from room temperature to the end of portlandite decomposition temperature (550 °C). As seen from Fig. 8(a), the CBW content of the reference was lowest at initial age and it increased rapidly after 2 h corresponding to the acceleration period of hydration. The change of CBW content for 30% S800 paste was consistent with the reference. Compared with the other two groups, 30% S600 paste was possessed of the highest initial content of CBW (around 5%). The CBW content increased mildly with age and was overtaken by the other two groups after 8 h. Interestingly, it was increased rapidly again at age of 24 h and exceeded that of the reference at 168 h.

The trend of portlandite content in the reference was similar as CBW. The rapid increasing period of portlandite content in the 30% S800 paste was prolonged as a delay of acceleration period for 4 hours. The gap (around 5%) in portlandite content between the reference and 30% S800 paste was enlarged after age of 24 h. As shown in Fig. 8, the portlandite content of the 30% S600 paste was lower than the other two groups and increased slowly, especially at the initial 24 hours of hydration. Subsequently, the

portlandite content entered a rapid accumulation period the same as the trend of chemical bound water.

The content of chemical bound water is corresponded to the amount of hydration products in cement paste. Based on the analysis of TG and XRD results, the high initial content of chemical bound water in the 30% S600 paste was resulted from formation of massive ettringite rather than the precipitation of portlandite. Subsequently, the tardy growth of chemical bound water and portlandite content were caused by inhibition effect of S600 on hydration of $C_3S$. It is worth noting that the XRD results (Fig. 6) showed an acceleration in the dissolution of $C_3S$ with the addition of S800 ash so the portlandite content was supposed to increase faster than that of the reference theoretically. However, the portlandite content of 30% S800 paste was lower at various age of hydration while the content of chemical bound water was on the contrary. It was evidenced that the pozzolanic reaction of S800 ash consumed a part of portlandite and generated more hydration products.

*3.3.3 BSE morphology*

The BSE images of the reference and the pastes with sludge ash are shown in Fig. 9. The various phases in BSE images can be discerned by morphological features and gray level depending on their mean atomic weight. Taking the reference paste as an example, the dark areas in the BSE image were pores and cracks, followed by C-S-H gel and other hydrated products such as ettringite and monosulfate. The bright parts were portlandite and unhydrated clinkers like $C_3S$, $C_2S$ and $C_4AF$. There were lots of partially hydrated clinkers in the cement paste after 7 days of hydration. The unhydrated core of clinker was wrapped by inner hydration products (IP) and the capillary pores were filled by outer hydration products (OP). The initial hydration products grew up without any space restriction resulting in a loose structure as seen in the BSE image. In the BSE images of 30% S600, only a small amount of C-S-H gel existed in the pores and no hydration product was attached to the surfaces of clinkers. The monosulfate phase was identified in the area with gray vertical cracks caused by the superposition of lamellar crystals. For the 30% S800 paste, the pores were filled fully by hydration

products leading to a compact structure. It was further proved that the pozzolanic reaction of S800 ash generated more hydration products and contributed to the development of microstructure.

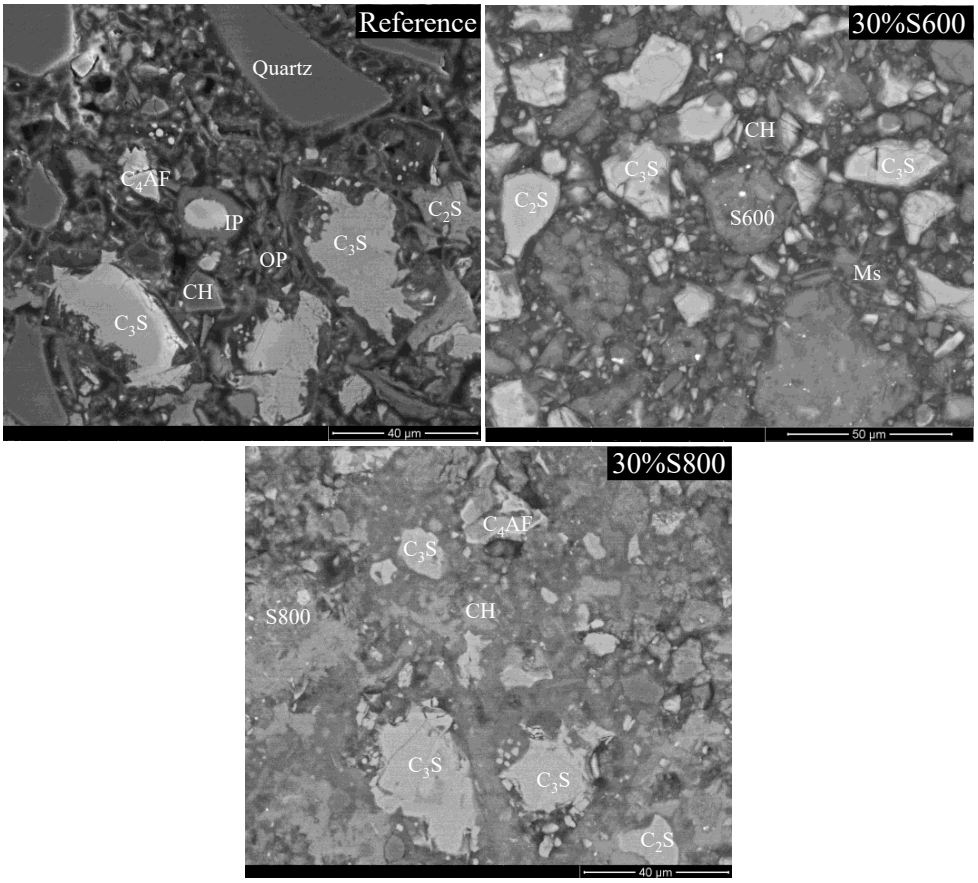


Fig. 9 The BSE images of paste samples at age of 7 days (IP=inner product, OP=outer product, CH=portlandite, Ms=monosulfate)

*3.4 Pore solution composition*

*3.4.1 Aqueous composition*

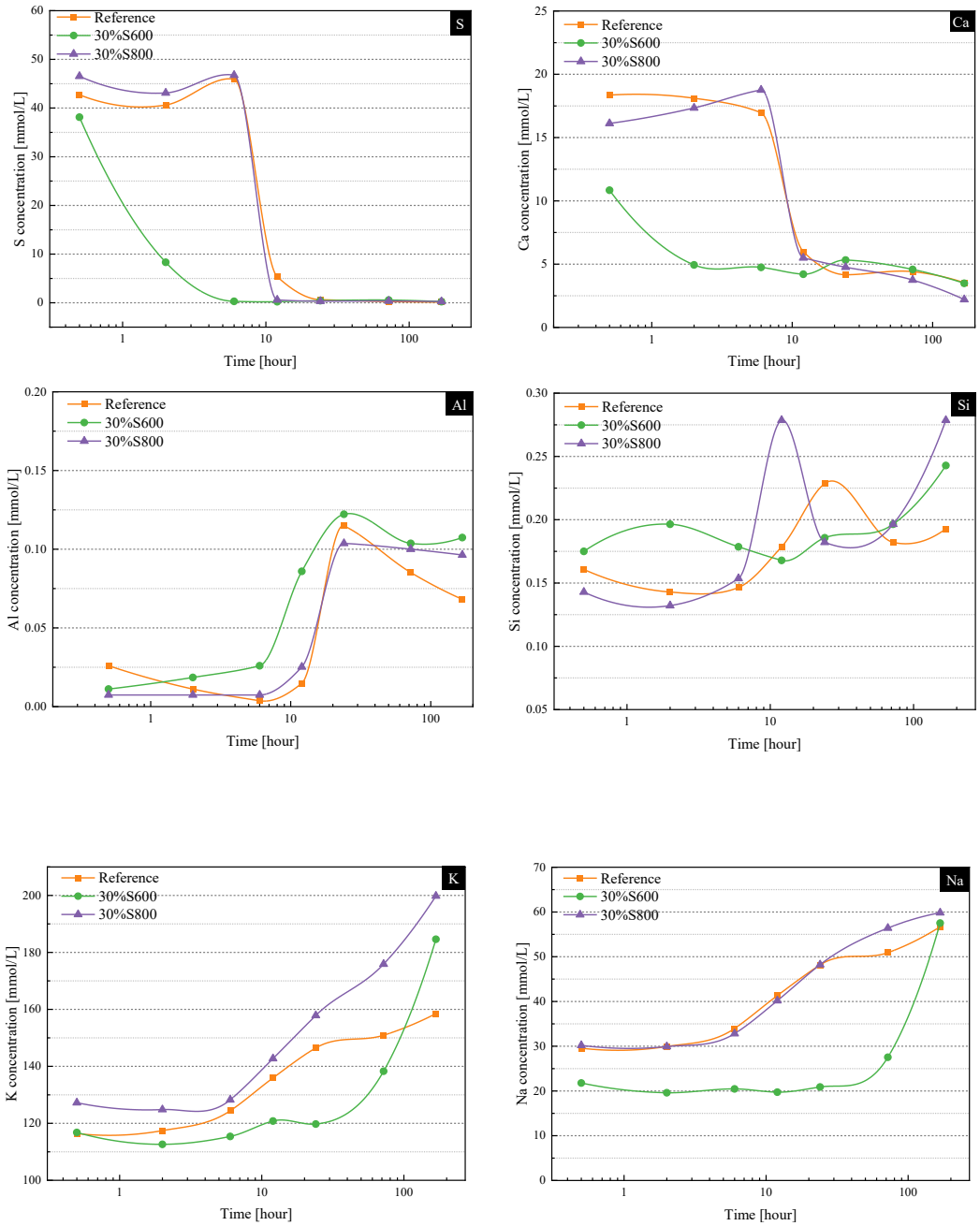


Fig. 10 Concentrations of S, Ca, Al, Si, K and Na in pore solutions at various hydration time.

The pore solution composition is dominated by Na, K, S, Ca and $OH^-$ at early age of cement hydration [43]. The ion concentrations in the pore solutions of the samples at different age are shown in Fig. 10. The rapid dissolution of the soluble sulfate and gypsum in cement resulted in a high initial concentration of $SO_4^{2-}$. A similar change

trend of $SO_4^{2-}$ concentration for the reference and 30% S800 paste was observed in Fig. 10. The $SO_4^{2-}$ concentration was maintained at 40~50 mM in the first 6 hour of hydration and dropped down rapidly in the next few hours. The $SO_4^{2-}$ concentration in pore solution of 30% S800 had fallen below 1 mM at age of 12 h. In comparison, the addition of S600 ash led to a decline of sulfate concentration in the first 6 hour corresponding to the early depletion of gypsum.

Ca ions in pore solution come from the dissolution of clinkers such as gypsum, $C_3A$ and $C_3S$. For the reference, the initial Ca concentration was 18.35 mM and was maintained above 15 mM in the first 6 hour of hydration. The precipitation of ettringite, C-S-H gel and portlandite from the solution reduced the Ca concentration. As shown in Fig. 10, the Ca concentration decreased rapidly in accordance with the change of $SO_4^{2-}$ concentration. The addition of S600 ash reduced the initial Ca concentration with a value of 10.84 mM. The depletion of gypsum and the inhibition on $C_3S$ dissolution decreased Ca concentration further in the first 2 hour.

In the reference paste, Al in pore solution was derived from the dissolution of $C_3A$. At the initial period of hydration, $SO_4^{2-}$ adsorbed on the surface of $C_3A$ and inhibited the dissolution of $C_3A$ resulting in a low initial Al concentration. The formation of ettringite generated from the reaction of Al, Ca and $SO_4^{2-}$ decreased Al concentration. The dissolution of $C_3A$ was accelerated by the depletion of gypsum. As can be seen from Fig. 10, the $SO_4^{2-}$ concentration had dropped to a low level after 12 h while the Al concentration increased rapidly at the same time. Subsequently the transformation of ettringite to monosulfate with the participation of Al caused a decline in Al concentration. For the pastes with sludge ash, the additional Al dissolved from sludge ash compensated the Al consumption at the initial time. The high Al dissolution degree of S600 ash led to an increase of Al concentration in the first 6 hour compared with the reference. The sustained-release Al maintained a high Al concentration above 0.1 mM after 24 h of hydration.

Si concentration in plain cement paste depends on the dissolution of $C_3S$ and the pH of solution at early age of hydration. No obvious change trend of Si concentration was found for three groups as shown in Fig. 10. The high concentration of Si in the 30%

S600 paste might be a result of less precipitation of C-S-H gel at initial age. The dissolution of amorphous Si in sludge ash also led to the increase in Si concentration after 72 h. The initial K and Na in pore solution is originated from the dissolution of sodium sulfate and potassium sulfate in cement. After 6 hours, alkali concentrations increased since the alkalis released from clinkers and the aqueous volume decreased. The low concentrations of K and Na in 30% S600 paste was related to its inhibiting effect on $C_3S$ dissolution.

The pH of pore solution at various hydration ages is shown in Fig. 10. For the 30% S600 paste, the early formation of massive ettringite consumed gypsum and sulfate resulting in a decrease of Ca and sulfate concentration in the solution. Meanwhile, hydroxide concentration increased in order to compensate charge balance. Correspondingly, the pH of solution rised rapidly in the first 6 hour. After 12 hours of hydration, the pH values of all solutions presented a similar change trend.

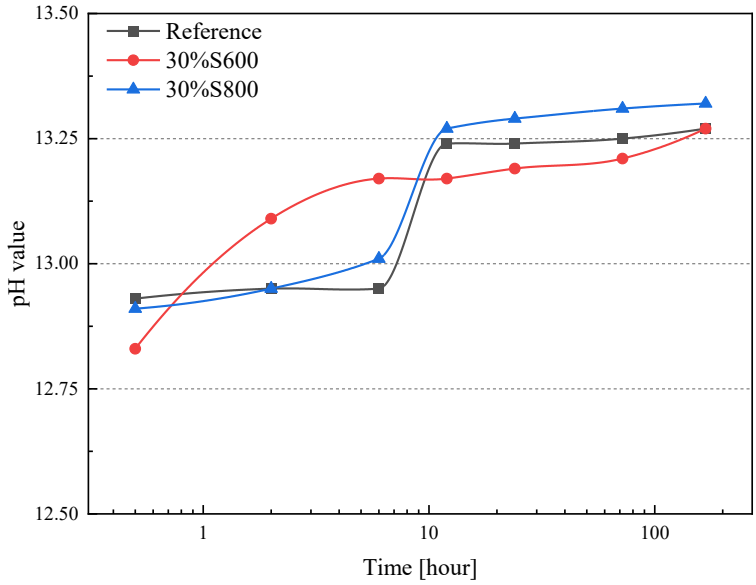


Fig. 11 The pH of pore solution at various hydration stages

*3.4.2 Effective saturation index*

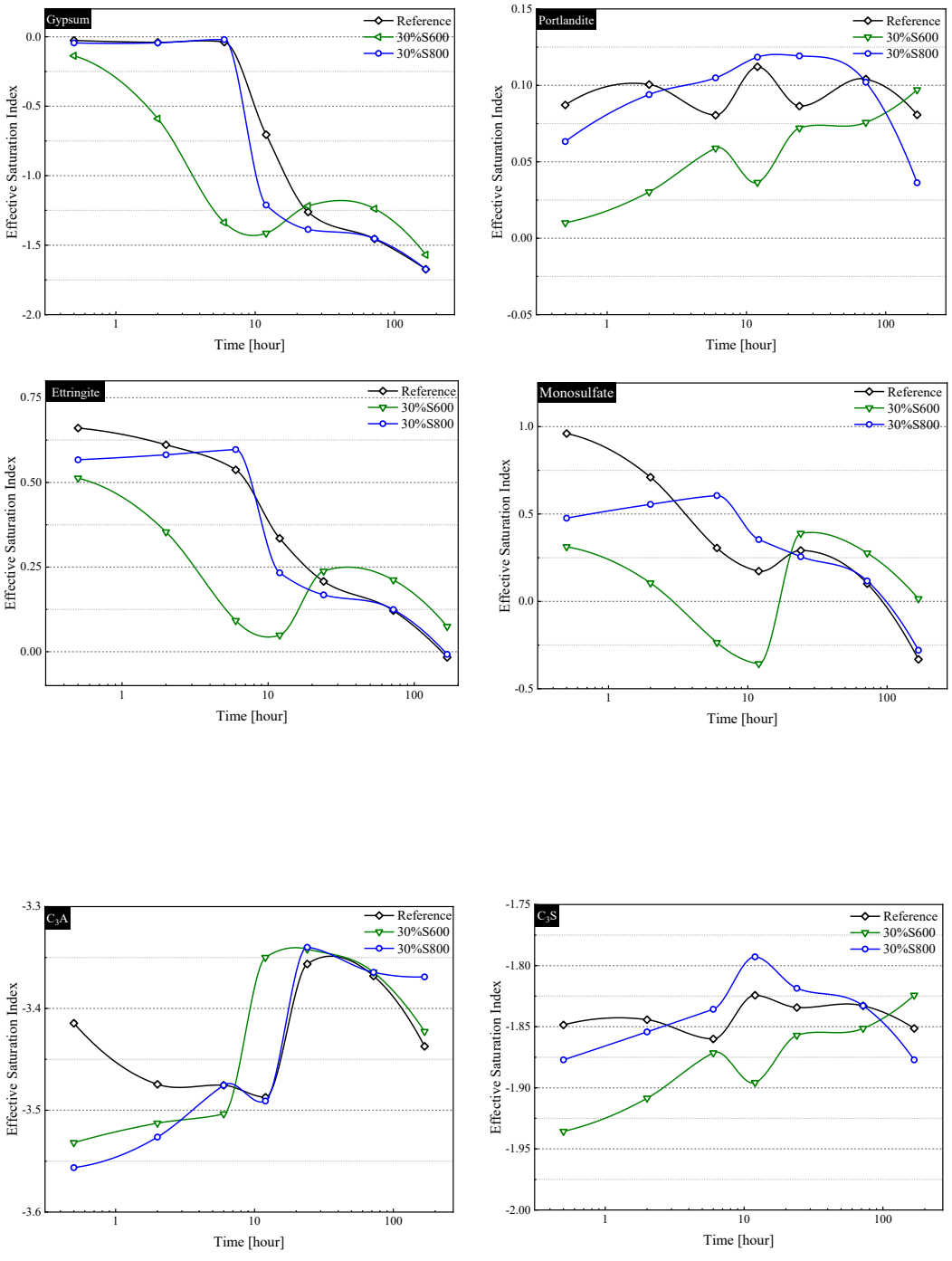


Fig. 12 Effective saturation index of different phases at various hydration stages

The saturation index (SI) of a solid phase is given by log (IAP/$K_{S0}$), where IAP is the ion activity product calculated from determined ion concentration in pore solution and $K_{S0}$ is the solid solubility product. A positive saturation index indicates

oversaturated for the respective solid and it tends to be precipitated. On the contrary, a negative value implies undersaturation for the respective solid which is inclined to dissolve. There are many solid phases in cement paste such as various hydration products and unhydrated clinkers. The existing state of a solid may be misled only in consideration of the saturation index since the various phases dissociate into a different number of ions. Thus, the effective saturation index ($SI_{eff}$) is introduced for the aqueous analysis which is calculated by SI/n, where n is the number of dominant ions dissociated from the respective phase.

The effective saturation index of key phases at different ages are shown in Fig. 12. The pore solutions were slightly undersaturated with respect to gypsum at initially. For the 30% S600 paste, the $SI_{eff}$ of gypsum decreased rapidly in the first 6 hour matching with the accelerated consumption of gypsum. As can be seen in Fig. 12, the solutions were always oversaturated with respect to portlandite. The initial $SI_{eff}$ of portlandite in 30% S600 paste was lower than the other two groups, resulting from the low Ca concentration at early age. All solutions presented a high initial $SI_{eff}$ of ettringite and the value decreased with the consumption of gypsum. Similarly, the solutions were also oversaturated to monosulfate and the $SI_{eff}$ decreased with time in the reference and 30% S800 pastes. As for cement clinkers, the addition of S600 and S800 ash reduced significantly the initial $SI_{eff}$ of $C_3A$ in the solution indicating that the early dissolution of $C_3A$ was accelerated in the presence of sludge ash. Despite inhibiting the dissolution of $C_3S$ by S600 ash, the calculated effective saturation index with respect to $C_3S$ was initially low attributing to the high Si concentration in the solution at the same time.

## 4. Discussion

The chemical effect of sludge ash on cement early hydration is dominantly by the dissolution of active Al and Si phases in ash which is related to the calcination temperature (Fig. 4) and the pH of solution [43]. The crystal structure and coordination number of Al phase can be changed during calcination process [44]. Higher calcination temperature reduces the defective sites of Al phase crystal resulting in a decrease of Al

activity [45]. This is the reason why the S800 ash presents a lower dissolution degree of Al compared with S600 ash. The pH values of pore solutions have exceeded 12.8 at 0.5 h of hydration and increased with time (Fig. 10). Al phase always exists in the form of $[Al(OH)_4]^-$ in alkaline solution (pH> 9) with a saturated concentration of $10^{-2}$ and $10^{-1}$ M. Al concentrations of pore solutions were measured between $10^{-5}$ M and $10^{-4}$ M far below the Al saturated concentration. Based on the analysis of solid and aqueous composition, the addition of sludge ash accelerates the early dissolution of $C_3A$ and at the same time the soluble Al in ash is dissolved into solution participating in the formation of ettringite. The dissolution and reaction process of active Al is shown in Eq. (1) (2):

$$Al_2O_3 \bullet xH_2O + 2OH^- \rightarrow 2Al(OH)_4^- + (x-3)H_2O \quad (1)$$

$$2Al(OH)_4^- + 6Ca^{2+} + 3SO_4^{2-} + 4OH^- + 26H_2O \rightarrow 3CaO \bullet Al_2O_3 \bullet 3CaSO_4 \bullet 32H_2O \quad (2)$$

Compared with the reference, the addition of S600 ash has a more significant effect on early cement hydration than S800 ash. As seem from the heat evolution curves (Fig. 5), the addition of S600 and S800 ash led to higher initial hydration heat of pastes in the first hour of hydration. The XRD pattern of 30% S600 paste showed a high diffraction peak of ettringite and diffraction peak of gypsum disappeared at age of 0.5 h (Fig. 6). Combined with a decrease in Ca and S concentration (Fig.10), it is indicated that the sludge ash promotes the early formation of ettringite with the participation of additional Al dissolved from ash. The high content of chemical bound water in the paste with 30% S600 ash at initial age also proves this point (Fig. 8).

After 6 hours, the hydration heat of the 30% S600 paste was almost stopped and the XRD pattern showed no obvious change on the diffraction peak intensity of $C_3S$. These phenomena illustrate that the addition of S600 ash inhibits the early dissolution of $C_3S$ significantly and results in a rather low rate of hydration heat. The inhibition effect of sludge ash on $C_3S$ hydration is attributed to the high Al and Si concentration and low Ca concentration in the solution. On the one hand, the dissolution of Al in sludge ash increases Al concentration in the first 6 hour of hydration. A previous study found that aluminum ions were covalently bound to the surface of $C_3S$ in the form of

aluminosilicate products rather than physical adsorption [46]. In addition, high Al concentration promoted the formation of Al-bearing C-S-H gel leading to a reduce of sites for C-S-H nucleation and growth [47]. The similar retard effect is observed in the study of Al-rich supplementary cementitious materials [41]. On the other hand, the early formation of massive ettringite accelerates the depletion of gypsum and the dissolution of $C_3S$ is inhibited by ash resulting in a low concentration of Ca (<10 mM) in the first hour. Subsequently, Ca concentration decreases further due to the continuous precipitation of ettringite. Thus, there is no additional Ca to participate in the formation of C-S-H gel and the precipitation of portlandite. Moreover, the dissolution of active Si in sludge ash increases Si concentration in pore solution which reduces the undersaturation of $C_3S$ and delays the dissolution of $C_3S$.

## 5. Conclusions

In this work, the physicochemical properties of sewage sludge ash calcined at 600 ℃ and 800 ℃and their chemical effects on the early-age hydration heat, solid and aqueous composition of cement paste were investigated. The following conclusions can be drawn based on the results and analysis:

(1) The main oxides of sewage sludge ash are $SiO_2$, $Al_2O_3$, $Fe_2O_3$ and a small amount of CaO. The amorphous phases such as Al and Si phase in sludge ash provide a material basis for potential pozzolanic activity. Under alkaline condition, the Al dissolution degree of sludge ash declines with calcination temperature due to a decrease of Al activity.

(2) The chemical effect of sludge ash on the early cement hydration is attributed to the dissolution of amorphous Al and Si phase. The additional Al dissolved from S600 ash accelerates the consumption of gypsum and $C_3A$ to form extensive ettringite at initial age of hydration. However, the high concentrations of Al and Si in the paste inhibit the dissolution of $C_3S$ significantly resulting in a rather low hydration exothermic rate.

(3) Considering the significant delaying effect of S600 ash on early cement hydration,

S800 ash is more feasible to be used as SCM. Even though the induction period of cement hydration is delayed by 4 hours, the subsequent pozzolanic reaction of amorphous phases in S800 ash with portlandite contributes to more hydration heat compared with the reference. Additional hydration products are filled into void space compacting the microstructure of cement paste. However, the long-term performance and durability of blended cement with sludge ash should be studied further.

## Acknowledgements

The authors gratefully acknowledge financial support from the Key R&D Projects of Hunan Province (Grant No. 2020WK2005) and the Postgraduate Scholarship, Central South University, Changsha, China.

## References

[1] A. Raheem, V.S. Sikarwar, J. He, W. Dastyar, D.D. Dionysiou, W. Wang andM. Zhao, Opportunities and challenges in sustainable treatment and resource reuse of sewage sludge: A review, Chem Eng J 337(2018) 616-641.10.1016/j.cej.2017.12.149

[2] A. Kelessidis and A.S. Stasinakis, Comparative study of the methods used for treatment and final disposal of sewage sludge in European countries, Waste Manage 32(2012) 1186-1195.10.1016/j.wasman.2012.01.012

[3] M. Schnell, T. Horst and P. Quicker, Thermal treatment of sewage sludge in Germany: A review, J Environ Manage 263(2020) 110367.10.1016/j.jenvman.2020.110367

[4] M. Praspaliauskas and N. Pedišius, A review of sludge characteristics in Lithuania's wastewater treatment plants and perspectives of its usage in thermal processes, Renewable and Sustainable Energy Reviews 67(2017) 899-907.10.1016/j.rser.2016.09.041

[5] L.G.G.D. Godoy, A.B. Rohden, M.R. Garcez, E.B.D. Costa, S. Da Dalt and J.J.D.O. Andrade, Valorization of water treatment sludge waste by application as supplementary cementitious material, Constr Build Mater 223(2019) 939-950.10.1016/j.conbuildmat.2019.07.333

[6] S. De Carvalho Gomes, J.L. Zhou, W. Li and G. Long, Progress in manufacture and properties of construction materials incorporating water treatment sludge: A review, Resources, Conservation and Recycling 145(2019) 148-159.10.1016/j.resconrec.2019.02.032

[7] Z. Chang, G. Long, J.L. Zhou and C. Ma, Valorization of sewage sludge in the fabrication of construction and building materials: A review, Resources, Conservation and Recycling 154(2020) 104606.10.1016/j.resconrec.2019.104606

[8] S. Donatello and C.R. Cheeseman, Recycling and recovery routes for incinerated sewage

sludge ash (ISSA): A review, Waste Manage 33(2013) 2328-2340.10.1016/j.wasman.2013.05.024

[9] C. Shi, A.F. Jiménez and A. Palomo, New cements for the 21st century: The pursuit of an alternative to Portland cement, Cement Concrete Res 41(2011) 750-763.10.1016/j.cemconres.2011.03.016

[10] M.C.G. Juenger and R. Siddique, Recent advances in understanding the role of supplementary cementitious materials in concrete, Cement Concrete Res 78(2015) 71-80.10.1016/j.cemconres.2015.03.018

[11] S.S.S.A. Nedunuri, S.G. Sertse and S. Muhammad, Microstructural study of Portland cement partially replaced with fly ash, ground granulated blast furnace slag and silica fume as determined by pozzolanic activity, Constr Build Mater 238(2020) 117561.10.1016/j.conbuildmat.2019.117561

[12] V.D. Katare and M.V. Madurwar, Design and investigation of sustainable pozzolanic material, J Clean Prod 242(2020) 118431.10.1016/j.jclepro.2019.118431

[13] A.L.G. Gastaldini, M.F. Hengen, M.C.C. Gastaldini, F.D. Do Amaral, M.B. Antolini andT. Coletto, The use of water treatment plant sludge ash as a mineral addition, Constr Build Mater 94(2015) 513-520.10.1016/j.conbuildmat.2015.07.038

[14] M. Coutand, M. Cyr and P. Clastres, Use of sewage sludge ash as mineral admixture in mortars, Proceedings of the Institution of Civil Engineers - Construction Materials 159(2006) 153-162.10.1680/coma.2006.159.4.153

[15] P. Garcés, M. Pérez Carrión, E. García-Alcocel, J. Payá, J. Monzó andM.V. Borrachero, Mechanical and physical properties of cement blended with sewage sludge ash, Waste Manage 28(2008) 2495-2502.10.1016/j.wasman.2008.02.019

[16] M. Mejdi, M. Saillio, T. Chaussadent, L. Divet and A. Tagnit-Hamou, Hydration mechanisms of sewage sludge ashes used as cement replacement, Cement Concrete Res 135(2020) 106115.10.1016/j.cemconres.2020.106115

[17] P. He, C.S. Poon and D.C.W. Tsang, Using incinerated sewage sludge ash to improve the water resistance of magnesium oxychloride cement (MOC), Constr Build Mater 147(2017) 519-524.10.1016/j.conbuildmat.2017.04.187

[18] Z. Chen and C.S. Poon, Comparative studies on the effects of sewage sludge ash and fly ash on cement hydration and properties of cement mortars, Constr Build Mater 154(2017) 791-803.10.1016/j.conbuildmat.2017.08.003

[19] M. Smol, J. Kulczycka, A. Henclik, K. Gorazda and Z. Wzorek, The possible use of sewage sludge ash (SSA) in the construction industry as a way towards a circular economy, J Clean Prod 95(2015) 45-54.10.1016/j.jclepro.2015.02.051

[20] M. Cyr, M. Coutand and P. Clastres, Technological and environmental behavior of sewage sludge ash (SSA) in cement-based materials, Cement Concrete Res 37(2007) 1278-1289.10.1016/j.cemconres.2007.04.003

[21] J. Monzó, J. Payá, M.V. Borrachero and I. Girbés, Reuse of sewage sludge ashes (SSA) in cement mixtures: the effect of SSA on the workability of cement mortars, Waste Manage 23(2003) 373-381.10.1016/S0956-053X(03)00034-5

[22] T.D. Dyer, J.E. Halliday and R.K. Dhir, Hydration Chemistry of Sewage Sludge Ash Used as a Cement Component, J Mater Civil Eng 23(2011) 648-655.10.1061/(ASCE)MT.1943-5533.0000221

[23] W. Piasta and M. Lukawska, The Effect of Sewage Sludge Ash on Properties of Cement Composites, Procedia Engineering 161(2016) 1018-1024.10.1016/j.proeng.2016.08.842
[24] Y. Liu, Y. Zhuge, C.W.K. Chow, A. Keegan, P.N. Pham, D. Li, J. Oh and R. Siddique, The potential use of drinking water sludge ash as supplementary cementitious material in the manufacture of concrete blocks, Resources, Conservation and Recycling 168(2021) 105291.10.1016/j.resconrec.2020.105291
[25] S. Donatello, A. Freeman-Pask, M. Tyrer and C.R. Cheeseman, Effect of milling and acid washing on the pozzolanic activity of incinerator sewage sludge ash, Cement and Concrete Composites 32(2010) 54-61.10.1016/j.cemconcomp.2009.09.002
[26] S. Naamane, Z. Rais and M. Taleb, The effectiveness of the incineration of sewage sludge on the evolution of physicochemical and mechanical properties of Portland cement, Constr Build Mater 112(2016) 783-789.10.1016/j.conbuildmat.2016.02.121
[27] T. Sopcak, L. Medvecky, M. Giretova, R. Stulajterova, J. Durisin, V. Girman and M. Faberova, Effect of phase composition of calcium silicate phosphate component on properties of brushite based composite cements, Mater Charact 117(2016) 17-29.10.1016/j.matchar.2016.04.011
[28] S. Donatello, A. Freeman-Pask, M. Tyrer and C.R. Cheeseman, Effect of milling and acid washing on the pozzolanic activity of incinerator sewage sludge ash, Cement and Concrete Composites 32(2010) 54-61.10.1016/j.cemconcomp.2009.09.002
[29] T. Wang, Y. Xue, M. Zhou, Y. Lv, Y. Chen, S. Wu and H. Hou, Hydration kinetics, freeze-thaw resistance, leaching behavior of blended cement containing co-combustion ash of sewage sludge and rice husk, Constr Build Mater 131(2017) 361-370.10.1016/j.conbuildmat.2016.11.087
[30] P.G.J.J. E. G. Alococel, Effect of sewage sludge ash (SSA) on the mechanical performance and corrosion levels of reinforced Portland cement mortars, Construction Materials 56(2006) 31-34
[31] Z. Chen, J.S. Li and C.S. Poon, Combined use of sewage sludge ash and recycled glass cullet for the production of concrete blocks, J Clean Prod 171(2018) 1447-1459.10.1016/j.jclepro.2017.10.140
[32] Y. Chen, T. Wang, M. Zhou, H. Hou, Y. Xue and H. Wang, Rice husk and sewage sludge co-combustion ash: Leaching behavior analysis and cementitious property, Constr Build Mater 163(2018) 63-72.10.1016/j.conbuildmat.2017.10.112
[33] O. Malliou, M. Katsioti, A. Georgiadis and A. Katsiri, Properties of stabilized/solidified admixtures of cement and sewage sludge, Cement and Concrete Composites 29(2007) 55-61.10.1016/j.cemconcomp.2006.08.005
[34] R. Li, W. Zhao, Y. Li, W. Wang and X. Zhu, Heavy metal removal and speciation transformation through the calcination treatment of phosphorus-enriched sewage sludge ash, J Hazard Mater 283(2015) 423-431.10.1016/j.jhazmat.2014.09.052
[35] Q.Y. Chen, M. Tyrer, C.D. Hills, X.M. Yang andP. Carey, Immobilisation of heavy metal in cement-based solidification/stabilisation: A review, Waste Manage 29(2009) 390-403.10.1016/j.wasman.2008.01.019
[36] B. Guo, B. Liu, J. Yang and S. Zhang, The mechanisms of heavy metal immobilization by cementitious material treatments and thermal treatments: A review, J Environ Manage 193(2017) 410-422.10.1016/j.jenvman.2017.02.026
[37] D. Wagner, F. Bellmann and J. Neubauer, Influence of aluminium on the hydration of triclinic $C_3S$ with addition of KOH solution, Cement Concrete Res 137(2020)

106198.10.1016/j.cemconres.2020.106198
[38] J. Zhou, K. Zheng, Z. Liu and F. He, Chemical effect of nano-alumina on early-age hydration of Portland cement, Cement Concrete Res 116(2019) 159-167.10.1016/j.cemconres.2018.11.007
[39] A. Souri, H. Kazemi-Kamyab, R. Snellings, R. Naghizadeh, F. Golestani-Fard and K. Scrivener, Pozzolanic activity of mechanochemically and thermally activated kaolins in cement, Cement Concrete Res 77(2015) 47-59.10.1016/j.cemconres.2015.04.017
[40] S.V. Vassilev, D. Baxter and C.G. Vassileva, An overview of the behaviour of biomass during combustion: Part I. Phase-mineral transformations of organic and inorganic matter, Fuel (Guildford) 112(2013) 391-449.10.1016/j.fuel.2013.05.043
[41] A. Schöler, B. Lothenbach, F. Winnefeld, M.B. Haha, M. Zajac and H. Ludwig, Early hydration of SCM-blended Portland cements: A pore solution and isothermal calorimetry study, Cement Concrete Res 93(2017) 71-82.10.1016/j.cemconres.2016.11.013
[42] H. Minard, S. Garrault, L. Regnaud and A. Nonat, Mechanisms and parameters controlling the tricalcium aluminate reactivity in the presence of gypsum, Cement Concrete Res 37(2007) 1418-1426.10.1016/j.cemconres.2007.06.001
[43] B. Lothenbach, G. Le Saout, E. Gallucci and K. Scrivener, Influence of limestone on the hydration of Portland cements, Cement Concrete Res 38(2008) 848-860.10.1016/j.cemconres.2008.01.002
[44] G. Busca, The surface of transitional aluminas: A critical review, Catal Today 226(2014) 2-13.10.1016/j.cattod.2013.08.003
[45] L. Kovarik, M. Bowden and J. Szanyi, High temperature transition aluminas in δ-$Al_2O_3$/θ-$Al_2O_3$ stability range: Review, J Catal 393(2021) 357-368.10.1016/j.jcat.2020.10.009
[46] L. Nicoleau, E. Schreiner and A. Nonat, Ion-specific effects influencing the dissolution of tricalcium silicate, Cement Concrete Res 59(2014) 118-138.10.1016/j.cemconres.2014.02.006
[47] F. Begarin, S. Garrault, A. Nonat and L. Nicoleau, Hydration of alite containing aluminium, Adv Appl Ceram 110(2013) 127-130.10.1179/1743676110Y.0000000007